Low-energy avionic piezoelectric deicing system

Modar Jomaa, Pierre-Etienne Lévy, Dejan Vasic, François Costa, Marwan Ali

Low-Energy Avionic Piezoelectric Deicing System

Modar Jomaa[1,4], Pierre-Etienne Lévy[1], Dejan Vasic[2], François Costa[3] and Marwan Ali[4]
1 Université Paris-Saclay, ENS Paris-Saclay, CNRS, SATIE, 91190 Gif-sur-Yvette, France
2 Université de Cergy-Pontoise, 95031 Cergy-Pontoise, France
3 Université Paris Est Créteil, INSPE, 94000 Créteil, France
4 Safran Tech, Groupe de Recherche E&E, 78117 Magny-Les-Hameaux, France

***Abstract*—Piezoelectric actuators are widely used in several applications and are becoming increasingly attractive in aircraft and industrial contexts, mainly when efficiency and economical energy conversion are required. One of these applications is the Avionic Piezoelectric Deicing System. Piezoelectric actuators are considered as a potential solution for developing a low-energy ice protection system for aircraft. This type of system applies vibration to the structure by activating its own resonant frequencies to generate sufficient stress to break the ice and cause it to delaminate from the substrate. The deicing mechanism depends strongly on the chosen excitation mode, whether it's flexural (bending) mode, extension (stretching) mode, or a combination in between, hence affecting the efficiency and effectiveness of the deicing process.**

However, it is essential to note that designing the power supply of the deicing system presents a major challenge, since piezoelectric actuators exhibit a distinct capacitive behavior in almost all frequencies, and eventually for deicing applications requiring high operational frequency.

In this contribution, a proof of concept of a deicing system utilizing lightweight piezoelectric actuators with minimal power requirement is proposed. Deicing was demonstrated with a power input density of 0.074 W/cm² and a surface ratio of 0.07 piezoelectric actuator per cm². First, a numerical method for positioning piezoelectric actuators and choosing the proper resonance mode was validated to assist in the system's design. Then, the numerical method was used to implement piezoelectric deicing on a more representative structure of an aircraft wing or nacelle. Finally, a converter topology adapted for deicing application was proposed.

***Keywords*—Deicing, piezoelectric actuator, extensional mode, resonant inverter, PWM inverter, soft-switching converter, reactive energy compensation.**

NOMENCLATURE

u	displacement, m
σ	stress tensor, Pa
λ	wavelength
c	wave propagation speed in the medium, m/s
n	resonant mode number
f	resonance frequency, Hz
ω	resonance angular frequency, rad/s
k	angular wave number
ε	strain tensor, Pa
E	Young's modulus, MPa
υ	Poisson's ration
ρ	volumetric mass density
L	plate length, m
PWM	Pulse Width Modulation
EMC	Electromagnetic Compatibility
ZVS	Zero Voltage Switching
ZCS	Zero Current Switching
GaN	Gallium Nitride

I. INTRODUCTION

ENVIRONMENTAL constraints and their impact on public opinion have led the aircraft industry to accelerate the energy transition in aeronautics towards a "More Electric Aircraft" (MEA). We are therefore witnessing a gradual increase in the role of electrical energy in onboard applications. This electrification trend aims to replace all non-propulsive systems (hydraulic and pneumatic) with electromechanical alternatives in order to optimize aircraft performance, decrease operating and maintenance costs, increase dispatch reliability, and reduce gas emissions. Among the systems underscored by this transition is the deicing system. Since ice accretion on aircraft wings and nacelles can significantly impact aerodynamic efficiency and balance, resulting in reduced lift and increased drag, aircraft require an ice protection system capable of meeting the demands of various certifications for full icing clearance. A variety of deicing methods, that defer by the energy used, are employed today to prevent ice formation. These include: turbine engine bleed air, pneumatic deicing boot system, chemical fluid, and electrically heated systems [1]. However, these methods are classified as very energy-consuming and are only suitable for some aircraft categories. Concerning electromechanical technologies such as electro-impulsive [2], electro-expulsive [3], and piezoelectric [4], the latter stands out as the most promising solution in terms of power consumption, weight, and cost effectiveness.

In the literature, different approaches using piezoelectric actuators have been explored. First it was investigated by Ramanathan et al [5], where experiments on resonant deicing systems were performed at very high frequencies to generate ultrasonic surface waves to produce shear stress at the ice/substrate interface. However, the deicing occurred through a thermal action. Experiments of deicing on low frequencies were carried out in the studies of Venna et al. [6], and Struggl et al. [7]. Yet, limited deicing performance. Kandagal and Venkatraman [8] partially deiced a simple flat plate with piezoelectric actuators by exciting resonant frequencies. Villeneuve et al. [9] worked on deicing a rotorcraft blade by studying actuator positioning and activation strategies. Partial deicing was achieved. Budinger et al. [10] compared different architectures of deicing based on piezoelectric actuators and on

the use of structural resonance modes. However, only tests with Langevin piezoelectric transducers were performed and where some delamination has occurred. In Budinger et al. [11], fracture mechanisms were analyzed. Key performance indicators were proposed to analyze the performance of such systems regarding fracture propagation.
This paper aims to produce a numerical model of a piezoelectric system in order to investigate crucial design parameters such as actuator positioning and sequencing, and then validate it through an experimental setup.
A converter topology adapted to piezoelectric actuators for deicing applications was selected and developed to drive the deicing system.

II. Piezoelectric deicing system

The operating principle of the piezoelectric deicing system is to create microscopic ultrasound mechanical vibrations based on the converse effect (reverse piezoelectric effect). Depending on the resonance mode, these electromechanical vibrations produce a stress field that initiates cohesive fractures in the ice, adhesive fracture at the interface leading edge/ice, or both [11]. Two configurations were introduced in the literature for using piezoelectric actuators. The first configuration with the Langevin transducer was used for its ease of installation using bolts, and the lower risk of mechanical failure due to their prestressed structure which allows them to withstand higher stresses during operation. However, the utilization of prestressed PZT ceramics, mainly designed to stimulate structural flexural modes, can, in the best cases result in some ice delamination [12]. This issue, coupled with their substantial weight, make them less advantageous. The second configuration with piezoelectric patches which can be glued to the mechanical structure was the most commonly tested in the literature and seemed to be more promising (**Erreur ! Source du renvoi introuvable.**).

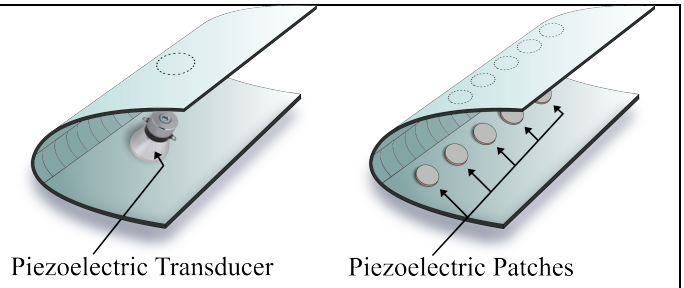

Fig. 1. Configuration of a piezoelectric de-icing system with piezoelectric patches and transducers.

A. Ice characterization

Numerous studies and experiments have been carried out to determine the adhesive and cohesive strength of ice on various materials and under diverse icing conditions [7] [13],[14],[15],[16],[17],[18]. These studies revealed that the expected adhesive shear strength value of refrigerated glaze ice can be estimated to be between 0.24 MPa and 1.7 MPa. The average adhesion shear strength of freezer ice to steel at -10°C was experimentally measured to be 1.5 MPa and the maximum was found to be at 1.66 MPa [19] while the cohesive tensile strength was found to be between [0.6 – 3] MPa [20],[21] [22]. Glaze ice characteristics are listed in table TABLE I.

TABLE I
Glaze Ice Characterization

Glaze ice	
Young's modulus (E)	9.3 GPa
Poisson's ratio (υ)	0.325
Density (ρ)	900 kg/m^3
Cohesive strength	[0.6 - 3] MPa
Adhesive strength	[0.24 – 1.7] MPa

B. Deicing mechanisms

The propagation of fractures after their initiation depending on the deicing mechanism has been stated in [23]. The first mechanism starts when tensile stress exceeds ice tensile strength leading to a cohesive fracture at the top of the ice layer which then propagates through the ice until the bottom at the ice/substrate interface. Consequently, adhesive fractures occur at this point, leading to ice delamination (Fig. 2). Cohesive fractures alone are insufficient for deicing as ice can stick to the surface on which it is accreted. Therefore, they should always be coupled with adhesive fractures to allow ice debonding.
The second mechanism starts when shear stress exceeds the ice/substrate interface shear strength leading to the initiation of an adhesive fracture and then the propagation of this adhesive fracture.
The examination of these two mechanisms has been conducted in the context of flexural and extensional modes. It has been shown that, in flexural modes, tensile stresses initiates fractures which is subsequently followed by cohesive and adhesive fractures [23], [24], whereas the second mechanism has been reported for extensional modes at high frequencies (32 kHz) [25], [26].
This contribution concentrates on the second mechanism of deicing using extensional modes.

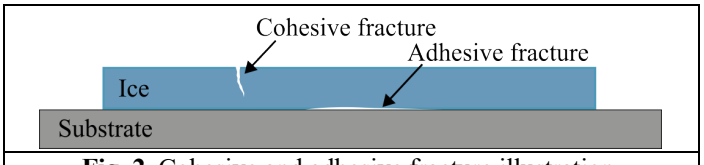

Fig. 2. Cohesive and adhesive fracture illustration.

C. Analytical and finite element analyses

In order to demonstrate the concept of piezoelectric deicing through the second fracture mechanism, validation of a numerical model of a piezoelectric deicing system applied to a simple flat plate structure had to be done. An aluminum alloy A5 1050 plate (150 mm × 50 mm × 1.5 mm) with one round hard PZT (PIC181) piezoelectric ceramic (ø 20 mm, 1 mm) bonded underneath in the center using epoxy resin, was modeled numerically in 3D using the finite element software COMSOL, its impedance was calculated and compared to the measured one (Fig. 3 & Fig. 4). The sample is held in free boundary conditions. The round shape of piezoelectric ceramic was chosen since it suffers less stress on the edges than a rectangular shape (any shape with angles) [27].

Since we are interested in the second fracture mechanism triggered by extensional modes, the latter is only being studied and tested. To simplify the problem, the actuator is considered to be as a point stress source and also displacements along the y and z axes will be neglected. This leads us to solve a one-dimensional problem.

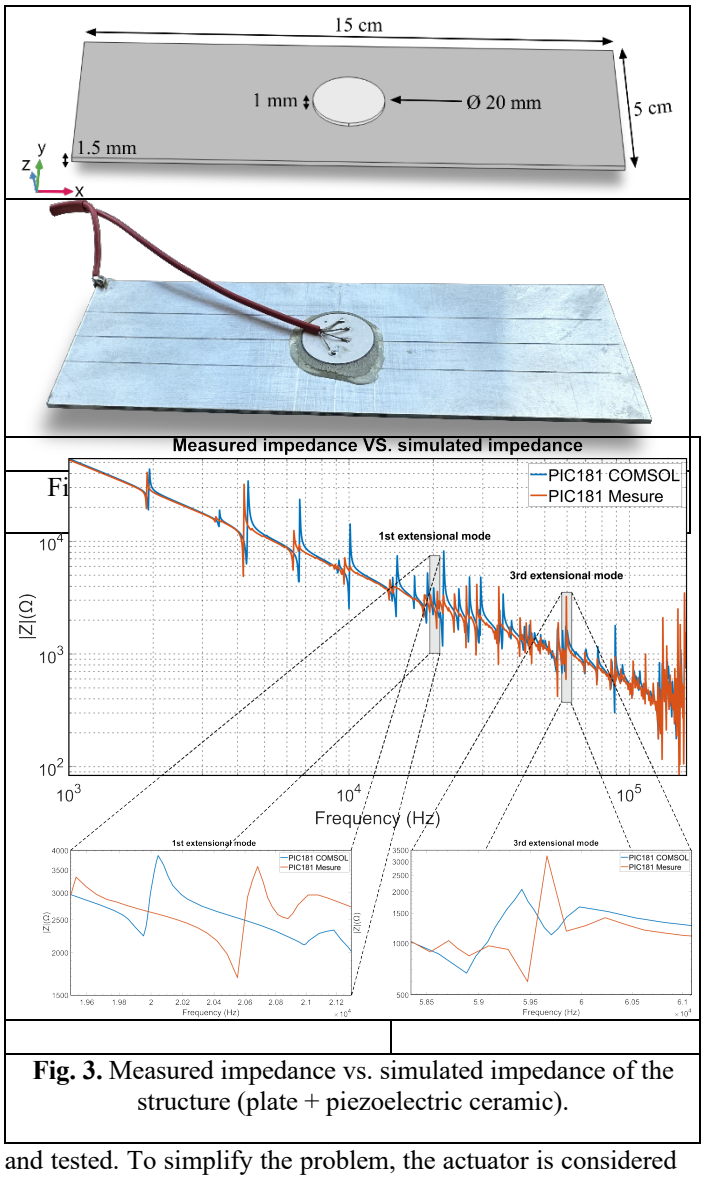

Fig. 3. Measured impedance vs. simulated impedance of the structure (plate + piezoelectric ceramic).

Wave equation:

$$\Delta\vec{E} = \frac{1}{C^2}\frac{\partial^2\vec{u}}{\partial t^2} \tag{1}$$

$$\frac{\partial^2\vec{u}}{\partial x^2} + \frac{\partial^2\vec{u}}{\partial y^2} + \frac{\partial^2\vec{u}}{\partial z^2} = \frac{1}{C^2}\frac{\partial^2\vec{u}}{\partial t^2} \tag{2}$$

Where $\vec{E}$ is the vector mechanical wave, $\vec{u}$ is the displacement vector and C is the wave propagation speed in the medium.

We are only looking for extension modes along the length of the plate:

$$\frac{\partial^2\vec{u}}{\partial x^2} = \frac{1}{C^2}\frac{\partial^2\vec{u}}{\partial t^2} \tag{3}$$

For a standing wave:

$$u(x,t) = f(x).g(t) \text{ with } \begin{cases} f(x) = \cos(kx + \Psi) \\ g(t) = \sin(\omega t + \varphi) \end{cases} \tag{4}$$

Derived Hooke's law for shear stress of a uniform bar:

$$\sigma = E.\varepsilon = E\frac{\partial u}{\partial x} \tag{5}$$

Since the plate has free boundary conditions:

$$\sigma(0,t) = 0\,, \sigma(L,t) = 0 \tag{6}$$

From (5) and (6):

$$\sin(\Psi) = \sin(kL + \Psi) = 0 \tag{7}$$

With $k = \frac{w}{c} = \frac{2\pi}{\lambda}$ is the angular wave number.

Then, from (7):

$$\Psi = 0 \quad \text{and} \quad \mathrm{kL} = \mathrm{n}\pi \tag{8}$$

Condition for the existence of a standing wave:

$$\lambda = \frac{2L}{n} \quad \text{with} \quad n \in \mathbb{R}^* \rightarrow f_n = \frac{n.c}{2L} \tag{9}$$

General stationary solution:

$$u(x,t) = \sum_{n=1}^{+\infty} A_n.\cos\left(\frac{n\pi}{L}x\right).\sin\left(\frac{n\pi}{L}c.t + \varphi_n\right) \tag{10}$$

$$\sigma(x,t) = \sum_{n=1}^{+\infty} B_n.\sin\left(\frac{n\pi}{L}x\right).\sin\left(\frac{n\pi}{L}c.t + \varphi_n\right) \tag{11}$$

Case 1: only one actuator

$$\begin{cases} \sigma(x_p,t) = \sigma_p.g(t) \\ \forall n, \quad \varphi_n = 0 \end{cases} \tag{12}$$

$$g(t) = \sin\left(N\pi\frac{c.t}{L}\right)$$

From (11) and (12):

$$\sigma_p.\sin\left(N\pi\frac{c.t}{L}\right) = \sum_{n=1}^{+\infty} B_n.\sin\left(\frac{n\pi}{L}x_p\right).\sin\left(\frac{n\pi}{L}c.t\right)$$

Then:

$$\begin{cases} n = N, & \sigma_p = B_n.\sin\left(\frac{N\pi}{L}x_p\right) \\ \forall n \neq N, & 0 = B_n.\sin\left(\frac{N\pi}{L}x_p\right) \end{cases}$$

Finally:

$$\sigma_p = \begin{cases} -1^{\frac{N-1}{2}}.B_n & if\ N\ odd \\ 0 & if\ N\ even \end{cases}$$

For this study case, only the fundamental extension mode and its odd harmonics will appear in the plate.

In simulations, in order to filter all other resonance modes except extension modes, zero displacements are imposed along the y and z axes. According to computations, the first extensional mode (fundamental) is found around 20 kHz which verifies the equation (9) where c = 6300 m/s for aluminum (Fig. 5).

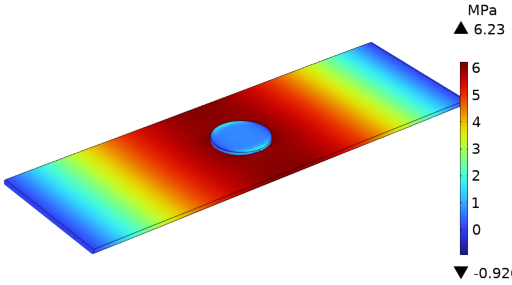

Fig. 5. Shear stress level at the 1st extension mode at 20 kHz with zero displacement imposed on the y and z axes.

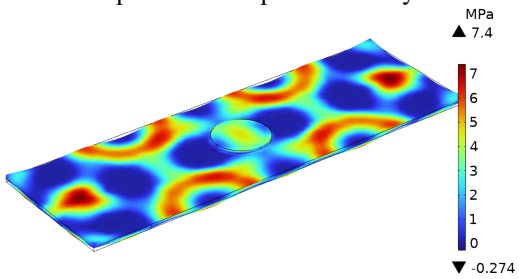

Fig. 6. Stress level at the 1st extension mode around 20 kHz with free displacement on the x, y and z axes.

However, when the displacement is set to be free on the three axes, the extensional mode will be coupled with flexural modes and other parasitic modes, making it difficult to be observable around 20 kHz (Fig. 6). At the first extensional mode coupled with other modes, stress level (shear + tensile) was not sufficient for cracking or debonding the 2 mm glaze ice layer and nothing happened experimentally. On the other hand, at the 3rd extensional mode around 60 kHz (Fig. 7 and Fig. 8), stress level (mainly shear stress) was higher, leading to some cohesive fractures but mainly adhesive fractures as illustrated in Fig. 9. In order to amplify the 3rd extensional mode, two other ceramics were bonded to the plate at the extensional wave crests as in Fig. 10.

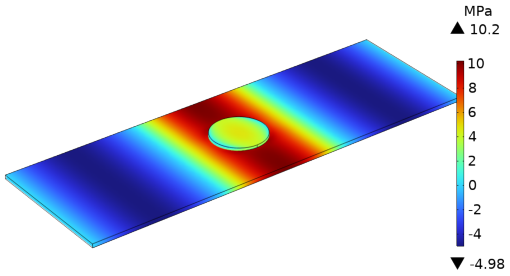

Fig. 7. Shear stress level at the 3rd extension mode at 59 kHz with zero displacement imposed on the y and z axes.

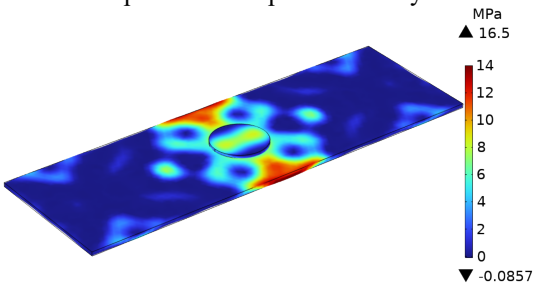

Fig. 8. Shear stress level at the 3rd extension mode at 59 kHz with zero displacement imposed on the y and z axes.

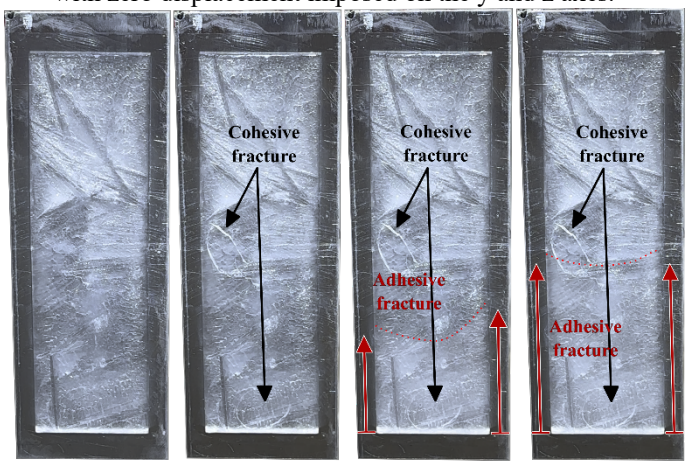

Fig. 9. Cohesive fractures and propagation of adhesive fracture at the 3rd extension mode.

Case 2: For three actuators placed at:

$$x_1 = \frac{L}{6}, x_2 = \frac{L}{2} \text{ and } x_3 = \frac{5L}{6} :$$

From (11) and (12):

$$\begin{cases} \sigma(x_1,t) = \sigma_1.g(t) \rightarrow \sigma_1 = B_1.\sin\left(n\frac{\pi}{6}\right) \\ \sigma(x_2,t) = \sigma_2.g(t) \rightarrow \sigma_2 = B_2.\sin\left(n\frac{\pi}{2}\right) \\ \sigma(x_3,t) = \sigma_3.g(t) \rightarrow \sigma_3 = B_3.\sin\left(n\frac{5\pi}{6}\right) \end{cases}$$

Were $B_1 = B_2 = B_3 = B$, since the three actuators are the same.

Then:

TABLE II

STRESS DISTRIBUTION BASED ON ACTUATOR POSITIONING AND THEIR FEEDING DIRECTION

n	σ_1	σ_2	σ_3	Feeding direction

1	$B/2$	B	$B/2$	↑ ↑ ↑
2	$B.\sqrt{3}/2$	0	$-B.\sqrt{3}/2$	↑ × ↑
3	B	$-B$	B	↑ ↓ ↑
4	$B.\sqrt{3}/2$	0	$-B.\sqrt{3}/2$	↑ × ↓
5	$B/2$	B	$B/2$	↑ ↑ ↑
6	0	0	0	× × ×

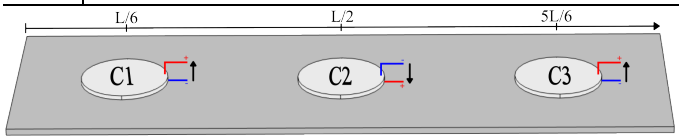

Fig. 10. Positioning and feeding direction of the three ceramics.

Feeding direction refers to the polarity of the applied voltage. The applied voltage on the three actuators will be like indicated in the 3rd case (mode 3) of Table TABLE II like indicated in Fig. 10. Computation results show as expected, a zero shear stress level for the first mode (Fig. 11) and a shear stress level approximately three times higher for the 3rd mode compared to when only one actuator is used (Fig. 12). As a result, we get in experimentation tests for the 3rd mode a multiple cohesive fracture at the beginning due to parasitic modes, followed by adhesive fractures and then a complete debonding of the ice. These three steps occur instantaneously at 200 V, taking place within a span of approximately 5 seconds as shown in Fig. 15.

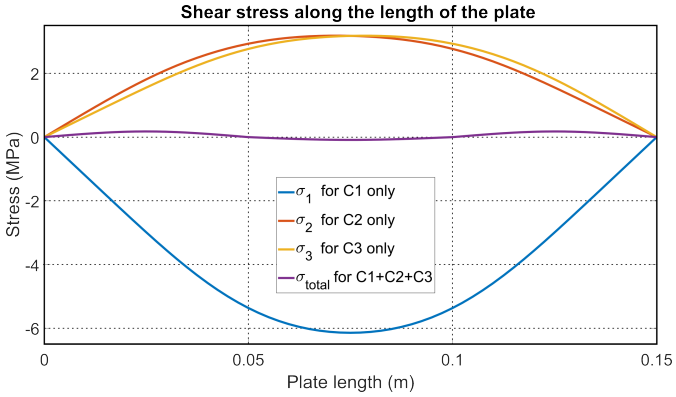

Fig. 11. Shear stress level traced along a line that runs the length of the plate at the 1st extension mode for one actuator at a time, and then all three together.

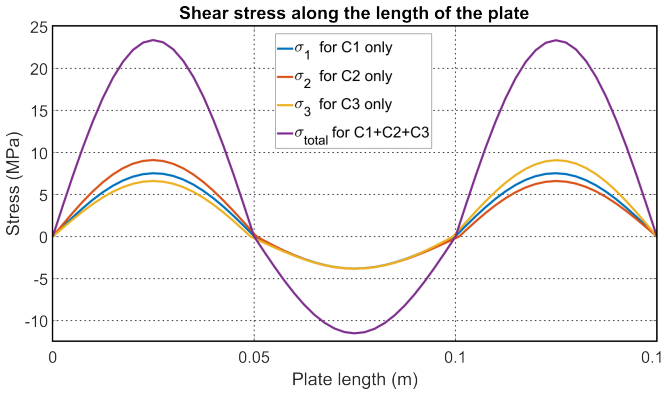

Fig. 12. Shear stress level traced along a line that runs the length of the plate at the 3rd extension mode for one actuator at a time, and then all three together.

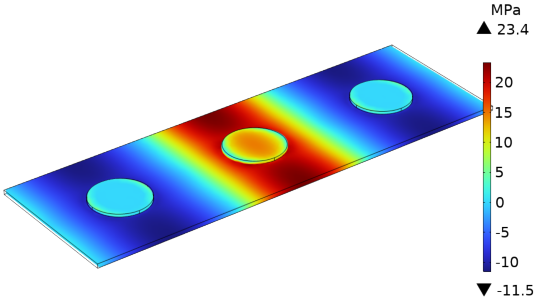

Fig. 13. Shear stress level at the 3rd extension mode at 59 kHz with zero displacement imposed on the y and z axes.

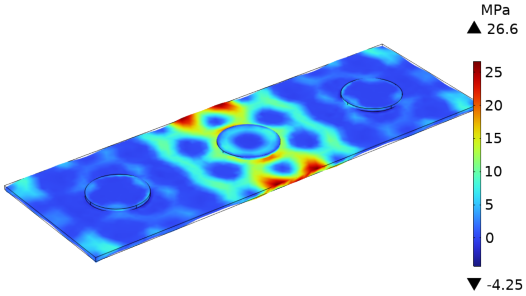

Fig. 14. Shear stress level at the 3rd extension mode around 59 kHz with free displacement on the x, y and z axes.

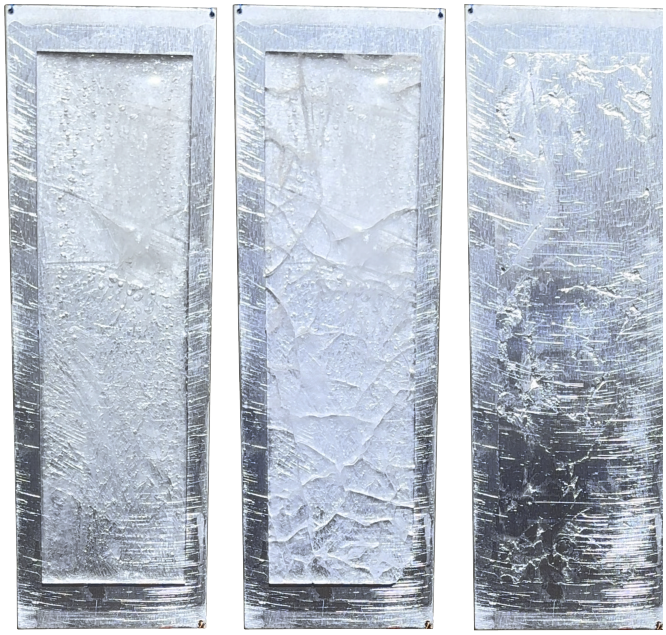

Fig. 15. Experimental result of deicing a 2 mm glaze ice layer at the 3rd extension mode of the rectangular plate.

Representative Model:

Following the validation of the numerical model of the small plate with the experimental setup, a more representative model was made. A large plate of aluminum of 350 mm × 250 mm × 1.5 mm dimension with 20 actuators with the same dimensions and material as used previously were employed to create the finale setup. The same strategy was used for driving and placing

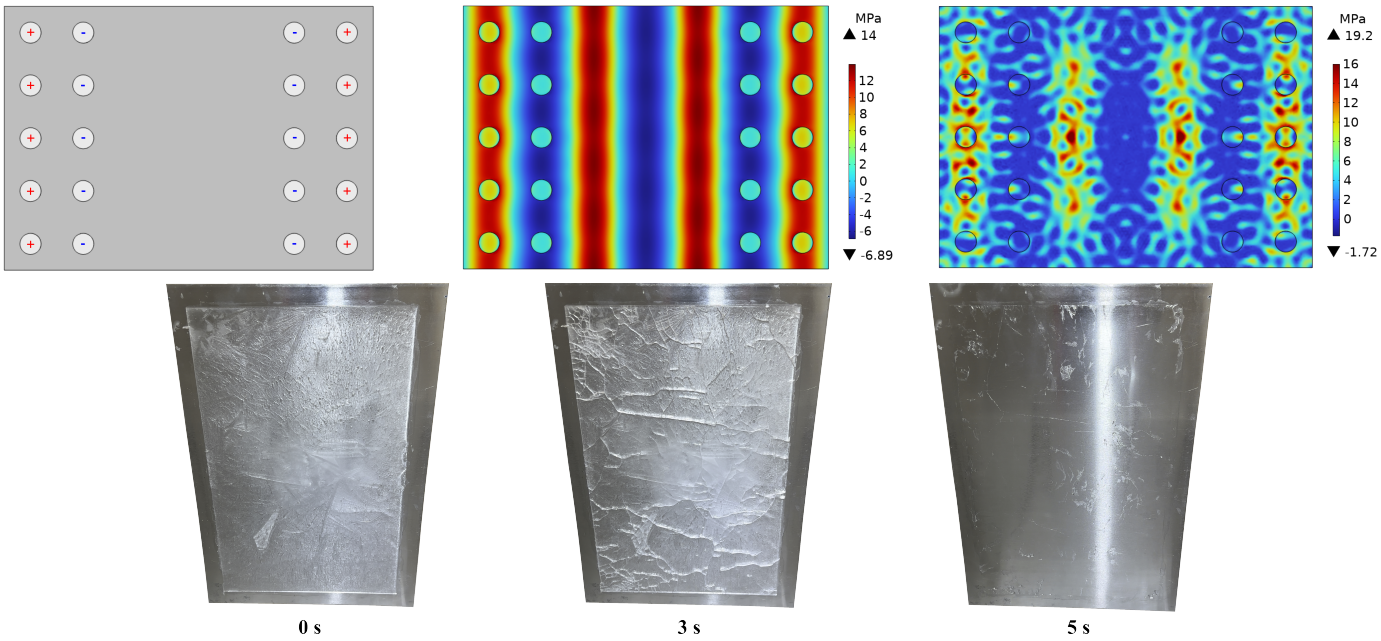

Fig. 16. Computation result of the 7th extension mode and its corresponding experimentation results.

the actuators. As illustrated in Figure 15, actuators were placed in a way to amplify the 7th extension mode at 55 kHz where we get enough stress and thus enough displacement to crack and delaminate the ice. At the same resonant frequency and with the same power by cm²?

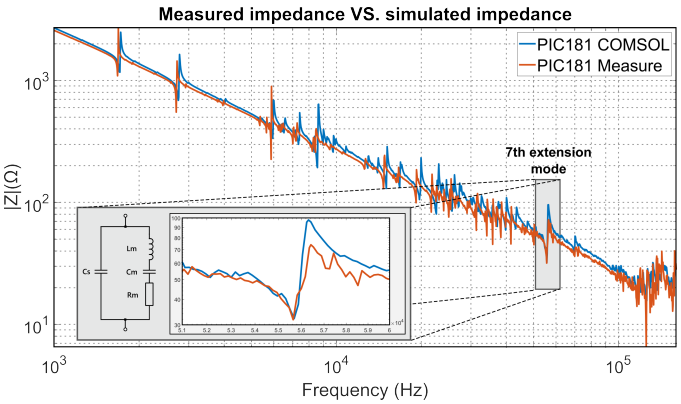

Fig. 17. Van Dyke circuit model of the setup in Fig. 16 around the 7th extension mode.

III. Electrical Specifications of the System

In order to properly drive a piezoelectric actuator and improve its performance, it is essential to know its electrical characteristics. The most common equivalent circuit that characterizes a piezoelectric actuator around its resonance frequency is the Van Dyke model. In this model, we identify the static capacitance Cs paralleled with a motional branch (Lm, Cm, Rm). Each piezoelectric actuator has several resonance frequencies in which its impedance has a lower magnitude as compared to non-resonance frequencies. To attain higher efficiency and deliver more power to the ultrasound system, actuators should be excited at their dominant resonance frequency which corresponds in our case to the 7th extension mode at 55 kHz (Fig. 17).

The deicing system and its power supply must comply with the aviation regulations and standards (DO 160), as well as the installation constraints of the equipment (safety, space requirements), while allowing its proper operation.

The power supply should deliver a sinusoidal voltage to the actuators in order to excite the desired mode. Otherwise, undesired harmonics (low-quality signal) can deteriorate the actuator's performance and increase power consumption in the system.

Finally, given the space constraints that do not allow to place the converter to be as close as possible to the load (actuators), the latter will be fed through 2 meters long cables (Fig. 18).

IV. Discussion on the Driving Power Supply for Optimized Feeding of the PZT Actuators State of the Art

Since the electrical behavior depends on the mechanical load and the temperature [27], it is essential to consider some aspects when designing the power supply. One is the driving frequency which must correspond to the mechanical resonance frequency of the actuators attached to the leading edge. In fact, at this resonance, the power transfer is better, and the reactive energy consumption is reduced (less losses). Another important aspect is the quality of the excitation signal, which has an important role in the piezoelectric actuator's performance and lifetime [28].

In this context, several techniques are proposed in the literature [29],[30],[31]. Linear power amplifiers (A, B, AB, ...) are used to feed piezoelectric loads because they can generate signals with low harmonic distortion rates. However, they have low efficiency and are often bulky and heavy. Therefore, switched-mode power supplies are more and more used and dominate the market because of their good efficiency and high-power density.

In this regard, various literature has focused on driving piezoelectric actuators using voltage source inverters. Resonant inverters (LC or LLCC) and PWM inverters (LC or LLCC) are the most commonly used. Other topologies have been used, such as the three-level NPC inverter and the current inverter [7]. The main disadvantages of resonant inverters are the volume and weight of the magnetic elements of the resonant filter and a very limited variation of the operating frequency. To overcome these drawbacks, PWM-controlled inverters (LC or LLCC) have been proposed [32]. The disadvantages of PWM control are often related to the switching frequency, which generates high switching losses and EMC (Electromagnetic Compatibility) problems. These issues can be particularly limiting in some cases, especially when GaN transistors are employed.

In [27], an investigation of three interesting topologies for driving ultrasound piezoelectric actuators under aeronautical constraints was conducted. The study revealed the predominance of the ARCPI (Auxiliary Resonant Commutated Pole Inverter) structure over the current source inverter (CSI) and the Energy Recovery "Resonant" structure.

AUXILIARY RESONANT COMMUTATED POLE INVERTER (ARCPI):

Several soft-switching inverter topologies have been proposed in the literature [33], [34], [35]. This type of inverter aims to achieve high-frequency operation with reduced switching losses and electromagnetic interference (EMI). An interesting example of soft-switching inverters of the "Resonant Pole Inverter (RPI)" family is the Auxiliary Resonant Commutated Pole Inverter (ARCPI) [36], [37],[38]. The circuit topology, and its theoretical waveforms, are illustrated in Fig. 20.

The inverter consists of two main arms and an auxiliary circuit connected to a capacitive divider bridge. In order to limit losses as well as the number of components, one arm is switched at Low Frequency (LF) synchronized to the transducer frequency, and the other is switched at High Frequency (HF), on which the auxiliary circuit is connected. The role of this circuit is to charge and discharge the parasitic capacitances C_{oss} to ensure ZVS condition on the HF arm. On the other hand, the control law of the auxiliary circuit implies zero current switching (ZCS) of its transistors. Moreover, since the auxiliary circuit is not in the main power path, the power rating of its switches will be reduced compared to that of the main switches. The control applied is a unipolar PWM which reduces the output voltage harmonics.

The experimental setup of the ARCP Inverter was built in the laboratory, as shown in Fig. 21, in order to drive the piezoelectric deicing system while respecting aeronautical constraints. The control of the inverter has been implemented in an FPGA to achieve a high precision on the driving frequency. The LF arm is switched at low frequency (55 kHz) synchronized to the output voltage while the HF arm is switched at high frequency at 2 MHz, under 270 Vdc bus voltage.

A more representative model of a wing's or nacelle's leading edge was created. An aluminum plate with the same dimension

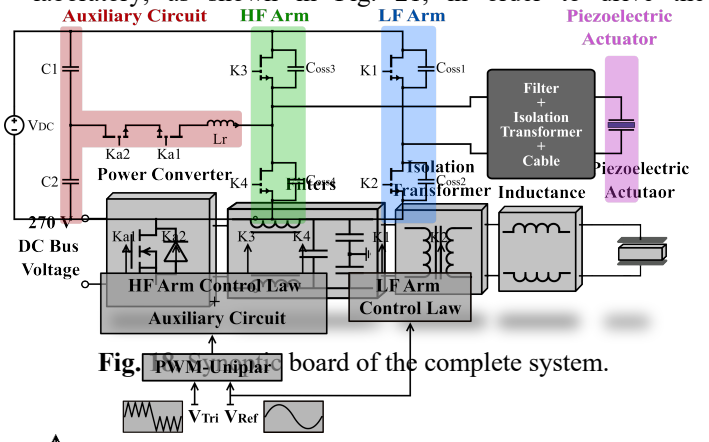

Fig. board of the complete system.

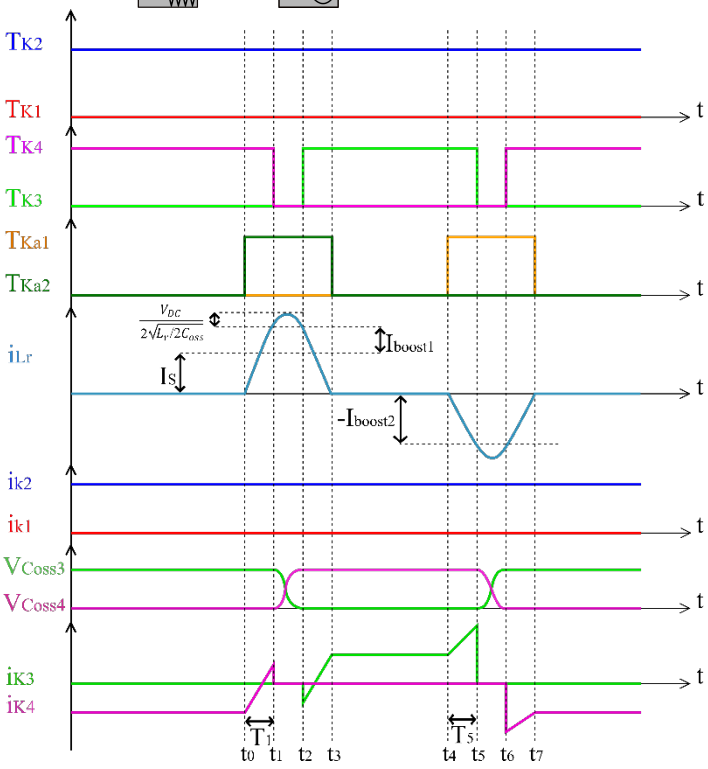

Fig. 19. ARCPI theoretical waveforms.

Fig. 20. Circuit topology of the ARCP Inverter.

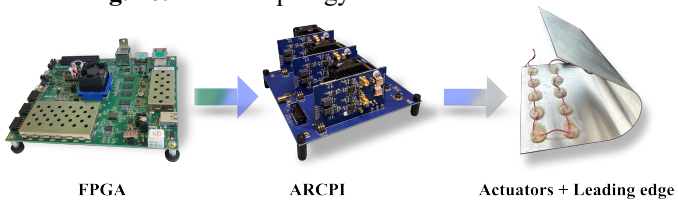

Fig. 21. Experimental setup of the complete deicing system.

as in figure 20 and the same number and distribution of actuators was used. The aluminum plate was then curved to replicate a section of a leading edge. With this new setup, we still have the 7th extension mode at 55 kHz.

At this frequency, an instantaneous cracking and delamination of 2 mm-thick-ice occurred with power input density of 0.074 W/cm² and a surface ratio of 0.07 piezoelectric actuators per cm². However, the driving power converter should be sized to deliver at least 0.41 VA/cm² o the actuators due to their capacitive behavior and the voltage level needed to initiate fractures in the ice.

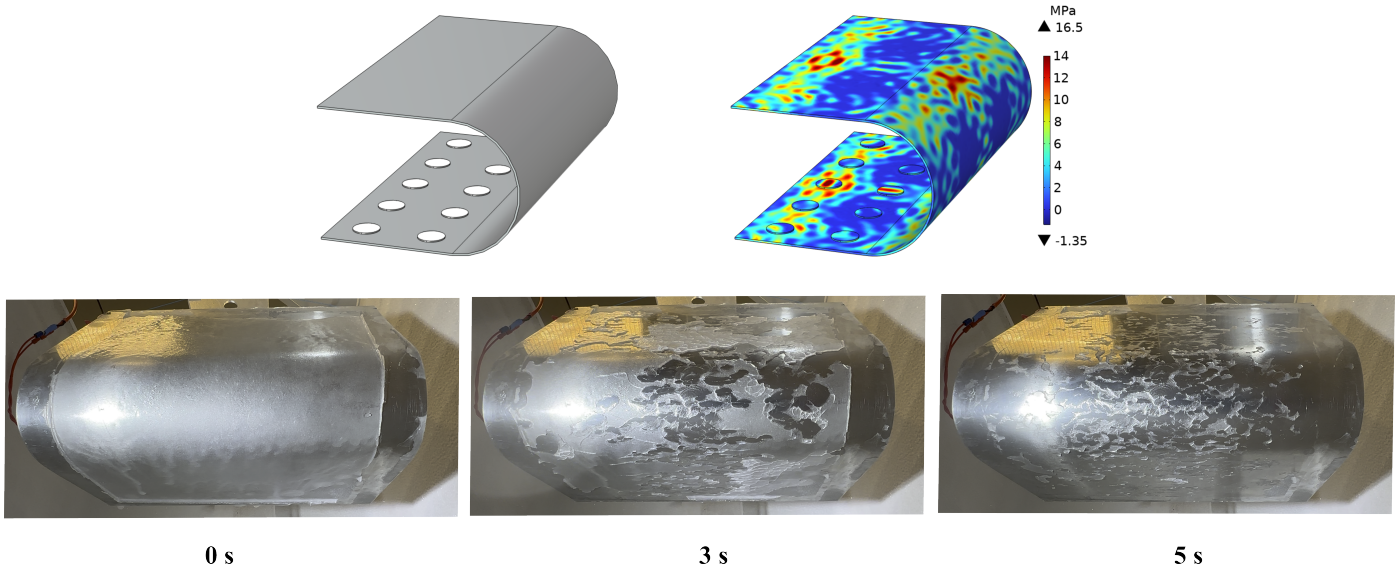

Fig. 22. Computation result of the 7th extension mode and its corresponding experimentation results.

CONCLUSION

The concept of deicing of wing's or nacelle's leading edge using piezoelectric actuators was demonstrated. Deicing was achieved using structural extension modes to ensure a sufficient shear stress level for ice delamination and complete deicing. It was shown through finite element simulation that it is difficult, and even impossible, to excite a resonance mode alone (extension or flexural) without having parasitic modes. This was confirmed through multiple experimentation tests where deicing always involved cohesive and adhesive fractures before achieving a complete deicing.

Analytical models, supported by COMSOL finite element simulations, were used to determine the proper excitation mode and the positioning of piezoelectric actuators.

A converter topology adapted to drive piezoelectric actuators was chosen and developed in the laboratory, through which, an adequate amount of power was delivered to ensure deicing. Experimental results showed complete deicing with a power input density of 0.074W/cm² and a ratio of 0.07 piezoelectric actuator par cm².

REFERENCES

[1] « Aviation Maintenance Technician Handbook - Airframe Volume 2 », p. 564.

[2] Robert D. Goehner, Norman I. Glover, et Donald G. Hensley, « ELECTRO-IMPULSE DE-CING SYSTEM FOR AIRCRAFT », 4,678,144, 7 juillet 1987

[3] Richard Alexander Olson et Mark Ronald Bridgeford, « ELECTRO-EXPULSIVE DE-CING SYSTEM FOR AIRCRAFT AND OTHER APPLICATIONS », US 2010/0288882 A1, 18 novembre 2010

[4] P. GONIDEC, J. RAMI, H. MAALIOUNE, R. BILLARD, V. RIGOLET, et J.-D. SAUZADE, « Methode for supplying electric power to a nacelle defrosting system and ice protection system through ultrasound », WO 2019/180361 A1, 26 septembre 2019

[5] S. Ramanathan, V. V. Varadan, et V. K. Varadan, « Deicing of helicopter blades using piezoelectric actuators », présenté à SPIE's 7th Annual International Symposium on Smart Structures and Materials, V. K. Varadan, Éd., Newport Beach, CA, juin 2000, p. 281-292. doi: 10.1117/12.388906.

[6] S. V. Venna, Y.-J. Lin, et G. Botura, « Piezoelectric Transducer Actuated Leading Edge De-Icing with Simultaneous Shear and Impulse Forces », J. Aircr., vol. 44, no 2, p. 509-515, mars 2007, doi: 10.2514/1.23996.

[7] S. Struggl, J. Korak, et C. Feyrer, « A basic approach for wing leading deicing by smart structures », présenté à SPIE Smart Structures and Materials + Nondestructive Evaluation and Health Monitoring, M. Tomizuka, Éd., San Diego, California, USA, mars 2011, p. 79815L. doi: 10.1117/12.880470.

[8] S. B. Kandagal et K. Venkatraman, « Piezo-Actuated Vibratory Deicing of a Flat Plate », in 46th AIAA/ASME/ASCE/AHS/ASC Structures, Structural Dynamics and Materials Conference, Austin, Texas: American Institute of Aeronautics and Astronautics, avr. 2005. doi: 10.2514/6.2005-2115.

[9] E. Villeneuve, D. Harvey, D. Zimcik, R. Aubert, et J. Perron, « Piezoelectric Deicing System for Rotorcraft », J. Am. Helicopter Soc., vol. 60, no 4, p. 1-12, oct. 2015, doi: 10.4050/JAHS.60.042001.

[10] M. Budinger, V. Pommier-Budinger, G. Napias, et A. Costa Da Silva, « Ultrasonic Ice Protection Systems: Analytical and Numerical Models for Architecture Tradeoff », J. Aircr., vol. 53, no 3, p. 680-690, mai 2016, doi: 10.2514/1.C033625.

[11] M. Budinger, V. Pommier-Budinger, A. Reysset, et V. Palanque, « Electromechanical Resonant Ice Protection Systems: Energetic and Power Considerations », AIAA J., vol. 59, no 7, p. 2590-2602, juill. 2021, doi: 10.2514/1.J060008.
[12] M. Budinger, V. Pommier-Budinger, G. Napias, et A. Costa da Silva, « Ultrasonic Ice Protection Systems: Analytical and Numerical Models for Architecture Tradeoff », J. Aircr., vol. 53, no 3, p. 680-690, mai 2016, doi: 10.2514/1.C033625.
[13] A. M. A. Mohamed et M. Farzaneh, « An experimental study on the tensile properties of atmospheric ice », Cold Reg. Sci. Technol., vol. 68, no 3, p. 91-98, sept. 2011, doi: 10.1016/j.coldregions.2011.06.012.
[14] S. R. J. et C. M. L., « Structural properties of impact ices accreted on aircraft structures.pdf ». 1 janvier 1987.
[15] P. H. Gammon, H. Kiefte, M. J. Clouter, et W. W. Denner, « Elastic Constants of Artificial and Natural Ice Samples by Brillouin Spectroscopy », J. Glaciol., vol. 29, no 103, p. 433-460, 1983, doi: 10.3189/S0022143000030355.
[16] U. Nakaya, « Visco-elastic Properties of Snow and Ice in Greenland Ice Cap ».
[17] J. Druez, C. L. Phan, J. L. Laforte, et D. D. Nguyen, « The Adhesion of Glaze and Rime on Aluminium Electrical Conductors », Trans. Can. Soc. Mech. Eng., vol. 5, no 4, p. 215-220, déc. 1978, doi: 10.1139/tcsme-1978-0033.
[18] J. J. Petrovic, « Review Mechanical properties of ice and snow ».
[19] « The adhesion and strength properties of ice », Proc. R. Soc. Lond. Ser. Math. Phys. Sci., vol. 245, no 1241, p. 184-201, juin 1958, doi: 10.1098/rspa.1958.0076.
[20] C. Laforte et J.-L. Laforte, « Deicing Strains and Stresses of Iced Substrates », J. Adhes. Sci. Technol., vol. 26, no 4-5, p. 603-620, mars 2012, doi: 10.1163/016942411X574790.
[21] F. Guerin, C. Laforte, M.-I. Farinas, et J. Perron, « Analytical model based on experimental data of centrifuge ice adhesion tests with different substrates », Cold Reg. Sci. Technol., vol. 121, p. 93-99, janv. 2016, doi: 10.1016/j.coldregions.2015.10.011.
[22] H. H. G. JeUinek, « ADHESIVE PROPERTIES OF ICE ».
[23] M. Budinger, V. Pommier-Budinger, L. Bennani, P. Rouset, E. Bonaccurso, et F. Dezitter, « Electromechanical Resonant Ice Protection Systems: Analysis of Fracture Propagation Mechanisms », AIAA J., vol. 56, no 11, p. 4412-4422, nov. 2018, doi: 10.2514/1.J056663.
[24] E. Villeneuve, C. Volat, et S. Ghinet, « Numerical and Experimental Investigation of the Design of a Piezoelectric De-Icing System for Small Rotorcraft Part 1/3: Development of a Flat Plate Numerical Model with Experimental Validation », Aerospace, vol. 7, no 5, p. 62, mai 2020, doi: 10.3390/aerospace7050062.
[25] J. L. Palacios et E. C. Smith, « Investigation of an Ultrasonic Ice Protection System for Helicopter Rotor Blades ».
[26] J. Palacios, E. Smith, J. Rose, et R. Royer, « Ultrasonic De-Icing of Wind-Tunnel Impact Icing », J. Aircr., vol. 48, no 3, p. 1020-1027, mai 2011, doi: 10.2514/1.C031201.
[27] M. Jomaa, D. Vasic, F. Costa, P.-E. Levy, et M. Ali, « Driving power supply for an avionic piezoelectric deicing system », in Active and Passive Smart Structures and Integrated Systems XVII, S. Tol, M. A. Nouh, S. Shahab, J. Yang, et G. Huang, Éd., Long Beach, United States: PIE, avr. 2023, p. 90. doi: 10.1117/12.2657036.
[28] Rongyuan Li, N. Frohleke, et J. Bocker, « LLCC-PWM inverter for driving high-power piezoelectric actuators », in 2008 13th International Power Electronics and Motion Control Conference, Poznan, Poland: IEEE, sept. 2008, p. 159-164. doi: 10.1109/EPEPEMC.2008.4635261.
[29] K. Agbossou, J.-L. Dion, S. Carignan, M. Abdelkrim, et A. Cheriti, « Class D amplifier for a power piezoelectric load », IEEE Trans. Ultrason. Ferroelectr. Freq. Control, vol. 47, no 4, p. 1036-1041, jul. 2000, doi: 10.1109/58.852087.
[30] H. L. Cheng, C. A. Cheng, C. C. Fang, et H. C. Yen, « Single-switch high power factor inverter for driving piezoelectric ceramic transducer », in 2009 International Conference on Power Electronics and Drive Systems (PEDS), Taipei: IEEE, nov. 2009, p. 1571-1576. doi: 10.1109/PEDS.2009.5385732.
[31] Sai Chun Tang et G. T. Clement, « A harmonic cancellation technique for an ultrasound transducer excited by a switched-mode power converter », in 2008 IEEE Ultrasonics Symposium, Beijing, China: IEEE, nov. 2008, p. 2076-2079. doi: 10.1109/ULTSYM.2008.0513.
[32] C. Kauczor et N. Frohleke, « Inverter topologies for ultrasonic piezoelectric transducers with high mechanical Q-factor », in 2004 IEEE 35th Annual Power Electronics Specialists Conference (IEEE Cat. No.04CH37551), Aachen, Germany: IEEE, 2004, p. 2736-2741. doi: 10.1109/PESC.2004.1355265.
[33] D. M. Divan, « The resonant DC link converter-a new concept in static power conversion », IEEE Trans. Ind. Appl., vol. 25, no 2, p. 317-325, avr. 1989, doi: 10.1109/28.25548.
[34] D. C. Katsis, J.-Y. Choi, D. Boroyevich, et F. C. Lee, « Drive Cycle Evaluation of A Soft-Switched Electric Vehicle Inverter », p. 6.
[35] J.-Y. Lim, J. Soh, et R.-Y. Kim, « An Improved Single-Phase Zero-Voltage Transition Soft-Switching Inverter with a Subtractive Coupled Inductor Auxiliary Circuit », in 2016 IEEE Vehicle Power and Propulsion Conference (VPPC), Hangzhou, China: IEEE, oct. 2016, p. 1-6. doi: 10.1109/VPPC.2016.7791610.
[36] R. W. De Doncker et J. P. Lyons, « The auxiliary resonant commutated pole converter », in Conference Record of the 1990 IEEE Industry Applications Society Annual Meeting, Seattle, WA, USA: IEEE, 1990, p. 1228-1235. doi: 10.1109/IAS.1990.152341.
[37] R. Teichmann et S. Bernet, « Investigation and comparison of auxiliary resonant commutated pole converter topologies », in PESC 98 Record. 29th Annual IEEE Power Electronics Specialists Conference (Cat. No.98CH36196), Fukuoka, Japan: IEEE, 1998, p. 15-23. doi: 10.1109/PESC.1998.701873.
[38] W. McMurray, « Resonant snubbers with auxiliary switches », IEEE Trans. Ind. Appl., vol. 29, no 2, p. 355-362, avr. 1993, doi: 10.1109/28.216544.

Modar JOMAA received his Engineering degree and Master's degree in Power Electronics from the ENSEEIHT engineering school and Paul Sabatier University, Toulouse, France, in 2020. He is currently working towards the Ph.D. degree with the French aeronautical group Safran, and SATIE laboratory, ENS Paris-Saclay, France. His research interests include power electronics for soft-switching inverters and related EMC in aeronautical applications.

Pierre-Etienne LÉVY received his Master's degree and his Ph. D from the Ecole Normale Supérieure de Cachan in France. He is currently working as an Assistant Professor in electrical engineering at ENS Paris-Saclay in France. His main research topics include power electronics converters and electromagnetic cpmpatibility.

Dejan Vasic obtained his agregation, master's, and doctoral degrees, all in electrical engineering, from the Ecole Normale Superieure de Cachan, France, in 1998, 2000, and 2003, respectively. He is currently a Full Professor of electrical engineering at CY Cergy Paris University, France, and his main research interests lie in the fields of piezoelectric materials for power electronics, dc–dc converters, energy harvesting, and structural damping.

François COSTA (member IEEE) received the Ph.D. in electrical engineering from the University Paris-Saclay, France, in 1992. He is a Full Professor in University Paris Est Créteil, France since 2003. He has been the responsible for the master degree in education in sciences & technology in the "Institut National Supérieur du Professorat et de l'Education (INSPE)" between years 2013 to 2019. From 2013 to 2019, he was also heading the "components & systems for electrical energy" department (CSEE) of lab SATIE (35 peoples, ~40 Ph.D. students). Since 2020, he is the director of the laboratory SATIE in university Paris-Saclay

His research fields include high-frequency medium-power converters, EMI issues and modelling, HF instrumentation, integration of power electronics, piezoelectric converters and low-level energy harvesting systems.

His main activities are focused on EMI in power converters and systems: multi-scales modelling of conducted and radiated emissions (from the component to the system), EMI filter design, EMI modelling of actuators, EMI measurement and characterization of wide bandgap semiconductors.